Solid Freeform Fabrication 2021: Proceedings of the 32nd Annual International
Solid Freeform Fabrication Symposium – An Additive Manufacturing Conference
Reviewed Paper

ANALYZING REMELTING CONDITIONS BASED ON IN-SITU MELT POOL DATA FUSION FOR OVERHANG BUILDING IN POWDER BED FUSION PROCESS

Zhuo Yang[1,2], Yan Lu[3,*], Brandon Lane[3,4], Jaehyuk Kim[2], Yande Ndiaye[2], Sundar Krishnamruty[1]

[1]Mechanical and Industrial Engineering Department, University of Massachusetts Amherst, Amherst, MA
[2]Associate at System Integration Division, National Institute of Standards and Technology, Gaithersburg, MD
[3]System Integration Division, National Institute of Standards and Technology, Gaithersburg, MD
[4]Intelligent Systems Division, National Institute of Standards and Technology, Gaithersburg, MD

Abstract

Coaxial melt pool monitoring (MPM) images provide in-depth insights into the building process of laser powder bed fusion additive manufacturing. An in-situ MPM image captures the independent melting condition at specific positions within each build layer. However, identifying material defects such as horizontal lack-of-fusion using individual, discontinuous MPM images poses multiple challenges. This paper builds upon the authors' previous work on data registration and data fusion to analyze material remelting conditions based on co-axial MPM images. MPM data are fused to formulate layerwise remelting 'maps' to evaluate printing quality. A 3D part with various overhang features was built to verify the method. A regular layer with solid support from the previous layers has around 30 % remelting ratio for the given laser scan conditions. In contrast, overhang regions remelted at about 10 % with the same process setting, whichis too low to provide sufficient material fusion, resulting in lack-of-fusion between melting tracks. The negative impact in remelting would not immediately disappear in subsequent layers following the overhang regions. Results shows three additional layers are required to fully recover the remelting condition back to normal. The remelting results from MPM are also visible within layerwise optical images of the same surface.

Introduction

Laser powder bed fusion (L-PBF) process uses laser to melt the powder spread on the build chamber. The material supplying mode in part formation is different than those additive manufacturing (AM) machines with a nozzle such as laser direct energy deposition (L-DED). Research shows the L-PBF can create parts of higher strength and ductility than L-DED [1], the random placement of particles in the powder bed itself introduces stochastic variability during the melting-solidification process [2]. In addition, variations in the laser beam, scan path, and build chamber environmental conditions introduce randomness that may cause irregular melt pool formation and lead to over-melting or under-melting [3, 4]. Complex geometric features add more difficulties in controlling melt-pool formation [5, 6]. However, defects associated with complex geometric features and process settings can potentially be predicted at the design stage, and, hence, they may be avoided during the process through re-design of process settings, or model-based feedforward control [6-8].

It is essential to understand the correlations between melting conditions and complex geometric features for defect prediction. For clarity, two concepts need to be explained – melting and remelting. Melting refers to the powder material initially changing from solid phase to liquid phase by receiving thermal energy from the laser beam [9]. The instantaneous molten region forms the melt pool, which traverses over specified areas of the powder layer using a prescribed scan strategy. The area over a powder layer that is traversed by the melt pool defines the solid portion of the AM part within that layer. It is critical to notice that the laser melts not only powders but also remelts previously solidified materials—either adjacent within the same layer, or remelts portions of the lower solidified layers. Remelting, as the name suggested, represents melting those previously solidified melt pools [10]. Remelting typically creates the overlapping region between adjacent melting tracks and establishes the consolidation of material within AM parts [11]. Defects, particularly lack-of-fusion porosity,

may occur when there is insufficient remelting, and is known to be a function of the melt pool geometry, the scan strategy, and the powder layer thickness [12]. On the other hand, excessive remelting may introduce different types of defects such as keyhole porosity, or heterogeneous microstructure [13, 14].

Figure 1 shows examples of different remelting conditions, conceptually. The figures are the cross-sections of two melting tracks. The dashed lines mark the laser beam center. The blue patches are remelting areas, and the orange circles are un-melted powders. The hatch spacing is the distance between the two tracks. Figure 1(a) demonstrates the normal remelting condition. The melt pool tracks have the ideal size and position to create just enough overlapping area between tracks and layers [15] leaving no un-melted powder. The resulting part would be fully dense once completely solidified. Figure 1(b) shows the under-melting condition while the melt pool itself has no initial defect. Insufficient remelting could be caused by poor scan strategy design, such as too wide hatch spacing, or layers that are too thick. Nevertheless, the under-melting in Figure 1(c) is mainly the result of irregular melt pools, or varying surface topography of the lower layer. The melt pool in Track 2 is significantly under-sized. As a result, it cannot establish enough overlap with Track 1, which has regular-sized melt pools. The small remelting area left un-melted powders around Track 1. These voids would form porosity in the final part. The causality of condition in (c) can be varied. On the other hand, oversized melt pool overlapping multiple times can cause over-melting condition. Common reasons for irregular melt pool formation are improper energy input that results in unstable melt pool formation (e.g., balling) [16], systematic fluctuations in local heating as a function of the scan strategy [7], or variations in local thermal conduction due to complex geometric features such as overhangs [8]. This paper chiefly focuses on the last condition—the impact caused by overhanging features.

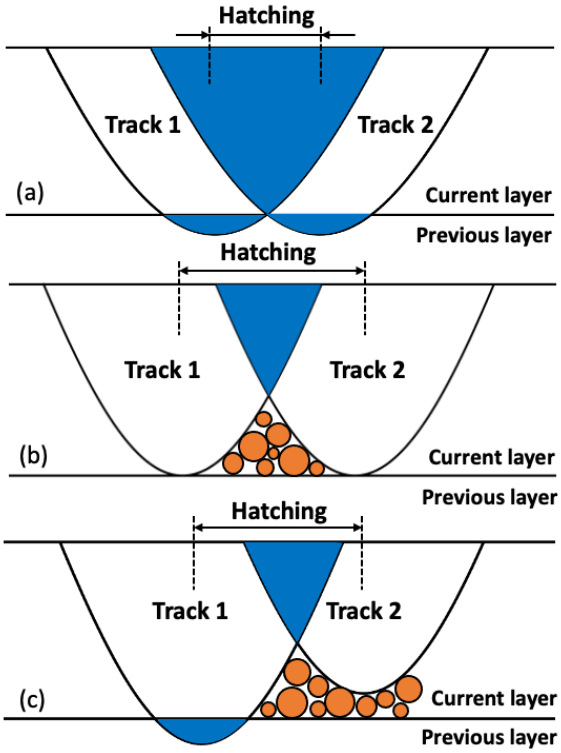

Figure 1. Conceptual remelting conditions between two melt pool tracks. Note, realistic melt pool geometries could be different. Blue patches represent remelting regions and orange circles are raw powder. (a) Proper melt pool size and hatch spacing create ideal remelting. (b) Abnormal remelting can happen while melt pool size cannot fill designed hatch spacing. (c) Irregular melt pool can cause abnormal remelting.

The overhanging surface is also called a 'downward-facing' surface or 'down-skin' surface [5, 17]. Instead of being supported by a solid layer, the overhanging surface is supported by powder. Most of the overhanging surfaces are created with purpose and specified by part geometry and build direction. Figure 2 shows an example of a typical overhanging surface. The cross-section of the part is on the left, where the dashed curve

is the overhanging surface. According to the layer-by-layer building process in L-PBF, the amplified view of the overhanging surface shows that the tip of each layer would always build on un-melted powders. The loose powder does not have the same strength as the dense solid. As a result, research shows that the overhanging region can exhibit defects such as craggy surface (or 'dross'), lower density, and inferior geometric deviation [5, 17].

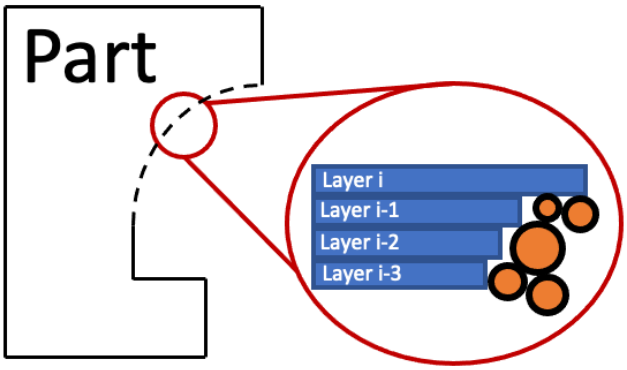

Figure 2. Overhang impact to powder bed fusion process.

Existing studies on overhang geometries built with AM are diverse in scope and methodology [17-20]. Simulations using finite element analysis or computational fluid dynamics mainly investigate the effect of heat accumulation in the vicinity of the melt pool due to the lower thermal conductivity of the powder compared to solid. Changes in surrounding material lead to locally variable thermal heat diffusion, and are prone to irregular melt pools on the overhanging region [5]. Experimental methods typically use traditional optical or mechanical measurement techniques to characterize AM overhang features. For example, scanning electron microscope (SEM) images show that residual pores are widely distributed in the overhanging region [5]. The rough overhanging down-skin surface has been characterized in various AM parts [21]. Those critical findings gathered evidence of the defects associated with overhang features. However, few studies examine what happens precisely during the build process or the physical conditions that lead to those defects. High-quality in-situ monitoring data may explain the transient states of the build process through advanced data analytics, which could undercover the causal relationships between overhang geometry, variable thermal conditions around the melt pool, and overhang defects [22].

This paper aims to analyze the remelting condition during the overhang build process based on high frequency in-situ monitoring data. This work designs a specific experiment that collects millions of in-situ monitoring images of a part with overhang features. We deploy the previously developed AM data registration [23, 24] and AM data fusion techniques [11] to reconstruct the remelting maps of L-PBF layers. The last two sections present and discuss the statistical and visualization results of the remelting conditions on overhang features.

Experimental Design

The Additive Manufacturing Metrology Testbed (AMMT) at the National Institute of Standards and Technology (NIST) is the primary platform developed to study powder bed fusion processes. AMMT is a fully customized metrology instrument that enables flexible control and measurement of the L-PBF process [25]. It is equipped with the capability of precise laser beam control and high-rate in-situ monitoring, including a coaxial camera with 10000 Hz maximum frame rate for melt pool imaging. The corresponding wavelength of the camera is 850 nm. Using custom-developed scan strategy design software, the digital commands that AMMT uses set precise laser beam position and laser beam power at 100 KHz, and synchronously triggers the MPM camera every 100 μs (or 10 KHz) [26].

Two types of in-process data can be acquired during the build on AMMT: pre-loaded digital commands and in-situ monitoring data. Digital commands construct the complete laser beam control, including timestamp,

laser beam position, laser power, and sensor trigger. The in-situ data includes layerwise images (LWI) and melt pool monitoring (MPM) images. LWI is the optical image of the surface of each layer, which can be used as a reference for recoated powder layer surface quality, or solidified surface quality [27]. MPM captures the coaxial melt pool images during the build with a resolution of 8 µm/pixel. Figure 3 shows the conceptual model of the AMMT and the sample data. Like the typical L-PBF process, the AMMT uses a galvo mirror scanner to steer and control the laser path. It also utilizes a custom-designed dynamic translating lens for laser flat-field correction, instead of an f-theta lens. This custom scanning lens is also optimized to enable diffraction-limited image quality for the MPM camera. The AMMT also employs a stationary LWI camera near the galvo mirror system, and flexible, multi-element illumination system. The LWI field of view covers the entire part surface, representing the final surface of each layer after powder recoating, and after the laser scan. MPM captures images of the incandescent light that radiates from the melt pool during the build. The white spot in the image center is the melt pool in the MPM example in Figure 3. Previous research published the calibration results between the MPM image grayscale values to the equivalent radiant temperature at the measured wavelength of 850 nm [28].

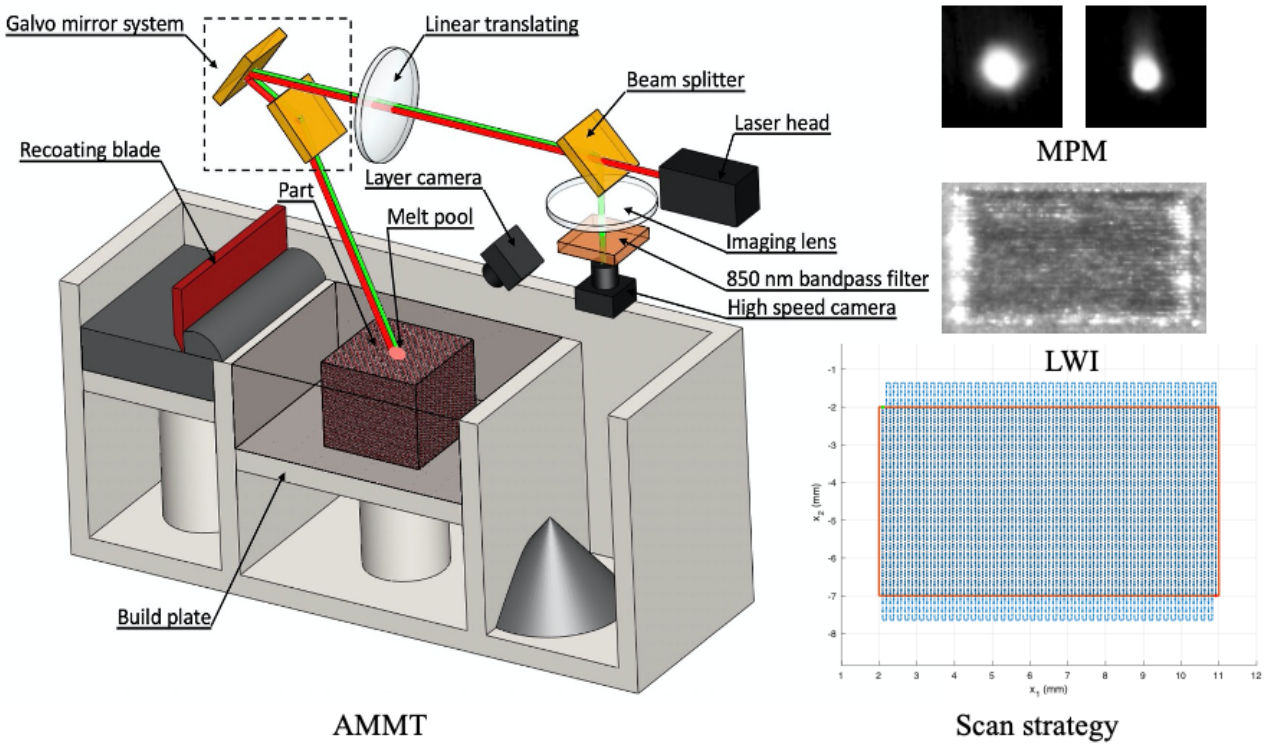

Figure 3. The AMMT uses different sensors to collect in-situ data: the coaxial MPM images, LWI, and scan commands.

For this study, an experiment is designed to create two types of overhanging features in one AM part. This experiment creates four nominally identical parts within the same build on a wrought nickel alloy 625 (IN625) substrate cut to 100 mm x 100 mm x 12.5 mm. All four parts have the same geometry: a bounding box 5 mm x 9 mm x 5 mm, a 45° overhang feature and a cylindrical cavity. The powder material is mixed recycled and virgin IN625 powder. The build consists of 250 layers at 20 µm per layer. The build employs a constant laser scan speed (800 mm/s) constant laser power (195 W). The scan strategy employs a stripe scan pattern with skywriting, and no pre- or post-contour scans. The general scan direction is designed to rotate 90° every layer. Detailed experiment descriptions can be found in [28]. Table *1* lists the properties of scan pattern and the abbreviation used in this paper.

Table 1. Description of the scan patterns used in this work. A 'vertical' or 'horizontal' scan track means the track is oriented in the Y or X direction, respectively. And, 'from right to left' or 'from top to bottom' means the tracks area scanned sequentially in the X or Y direction.

	Scan Pattern	Name
Layer 1, 5, 9, …	Vertical scan track from right to left	V-R2L
Layer 2, 6, 10,…	Horizontal scan track from top to bottom	H-T2B
Layer 3, 7, 11, …	Vertical scan track from left to right	V-L2R
Layer 4, 8, 12, ….	Horizontal scan track from bottom to top	H-B2T

Figure 4 shows the designed part dimensions and the key geometric features. This paper focuses on the overhang surface on top of the cylindrical hole feature with 3 mm depth. Figure 4(b) is the cross-sectional view of the part in YZ plane at a point along the axis of the cylindrical feature. As shown, the overhang feature is introduced at Layer 126 and gradually developed until Layer 226. The red line marks the pure overhang surface on Layer 226. The solid and dashed lines indicate the infilling (laser on) and non-infilling (laser off) regions, respectively.

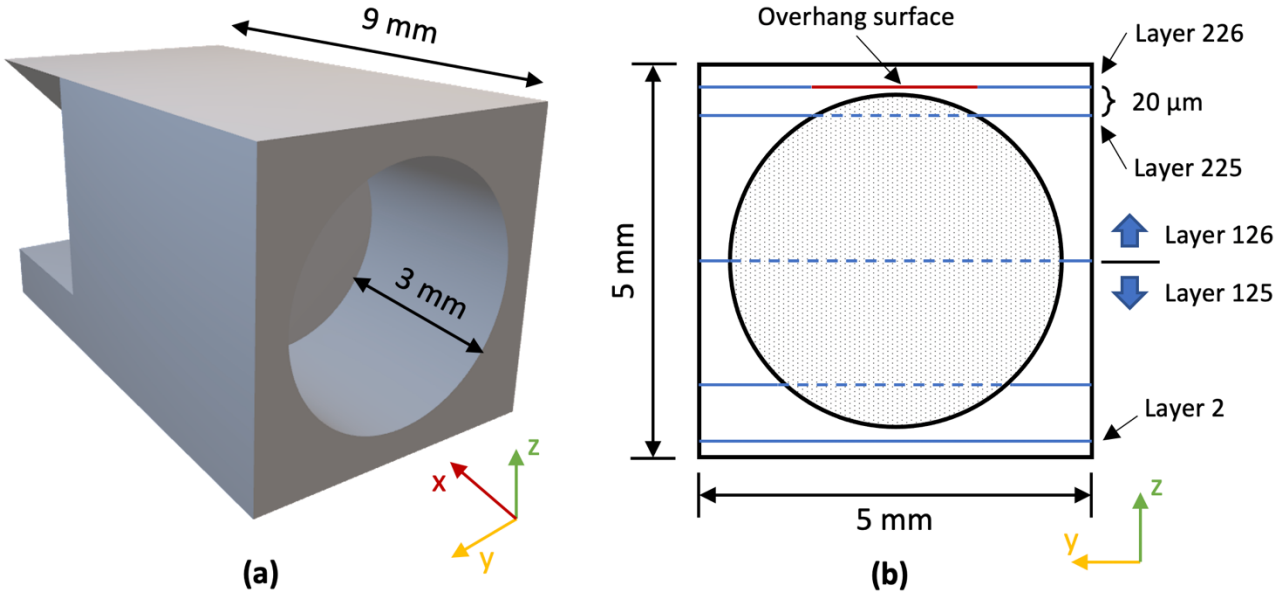

Figure 4. The part dimensions and key geometric features. (a) the 3D model showing a horizontal cylindrical feature on one side of the part with 3 mm depth (and 4 mm diameter). (b) is cross-sectional plane showing relative layer positions. Solid lines represent the infilling region (laser on). Dashed line is the non-infilling region (laser off). The shaded region indicates un-melted powders within the hole. The initial overhang surface is red line on Layer 226.

The following sections explain how MPM data are used to create remelting maps for overhang build process study. For demonstrative purposes, this study only studies the overhang associated with the cylinder hole using the data from one part.

Method

In this section, we will introduce the method of creating a layerwise remelting map using in-situ MPM data. Figure 5 shows the general workflow of this procedure. It starts with data preprocessing to clean the raw data. Data registration is the second step to synchronize and align the data from various sources. Data fusion is the next step. The objective is to integrate the multimodal data into one indicator by applying various rules that depend on the purposes of the fusion, and/or the physical meanings of the data. After that, the fused AM data could be used for mapping the remelting conditions of each layer. The final step is to calculate the remelting ratio.

The first step is to preprocess the raw data, which includes correcting the signal delay in digital command and removing noise from the raw MPM images. The signal delay is measured from sensor and machine calibrations [26]. Two features in the melt pool measurement are removed in data preprocessing: the background or dark-level noise, and the effect of plumes and spatters. A low threshold grayscale value, 20 in this work, is deployed to remove the background noise. The largest connected area (LCA) method is used to remove the spatters in the MPM images. Observations found that spatters typically have much smaller sizes than melt pools where they originate. After the LCA filter, each melt pool image only contains one large white spot – the melt pool.

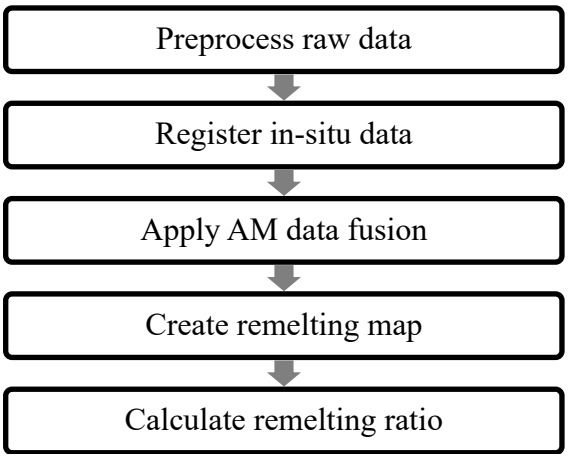

Figure 5. Workflow for calculating the remelting ratio.

Data registration is a concept in which data from various sources are synchronize or aligned within the same temporal or spatial domain. Spatial registration procedures transform different datasets to a single coordinate system [23]. The authors' previous works developed an AM specific data registration method to register the pixels in each MPM image to a global coordinate system [24]. Detailed procedures could be found in Feng et al 2021 and Lu et al 2020 [24, 29]. The registration maps the MPM image files to the commanded scanning position, which is defined in the AM machine and laser's coordinate system. The registered MPM information still requires further processing conducted by users based on specific application needs. However, the MPM data fusion step plays a role in providing physical meanings to the MPM data by matching it to the spatial location within the part where and when each melt pool image was captured.

Data fusion, as it stated, is "a technology to enable combining information from several sources in order to form a unified picture" [30]. It has been commonly used in defense but rare in manufacturing due to the lack of rich data types. New technological improvements continually increase the quantity of AM in-situ data acquired by built-in sensors and controllers [25]. Applying data fusion methods can provide advantages to this data-heavy AM domain. A multi-scale hierarchical AM data fusion method was recently introduced and demonstrated to address specific AM problems [11]. It fuses AM in-process raw data in pointwise, trackwise, layerwise, and partwise levels. Melting condition considered in this paper is mainly investigated with the spatial alignment at trackwise level. The next few paragraphs introduce the algorithm used to create remelting maps based on this AM data fusion strategy.

Melt pool width and hatch spacing are two critical factors of remelting. Hatch spacing is a process parameter preconfigured during scan strategy development before the build starts. For a fixed hatch spacing, wider melting tracks have a higher chance to create more overlapping and remelting. Conversely, for a fixed melt pool width, wider hatch spacing decreases overlapping and remelting. The melt pool width can be directly measured after the build, which being verified in many single-track experiments [31]. However, it is not easy to measure the actual melt pool width from in-situ images in a multi-track layer. The actual melting and solidification

temperature may only be identified with a thermally calibrated imager [32, 33]. Figure 6 shows an example of melt pool width measurements based on different threshold values, and the imager pixel scaling of 8 μm/pixel. The left chart shows the width measured using different threshold grayscale values, and the right figure is an MPM image with a melt pool moving vertically from top to bottom. While increasing the threshold value, larger areas within the melt pool image are removed (or set to binary value 0), and remaining areas of binary value 1 decrease in size. In this example, the thresholded region corresponding to the melt pool 'tail' becomes less elongated after threshold value of 150. Results in the rest of this paper are based on grayscale threshold 80, which is consistent to the authors' previous work [4, 6].

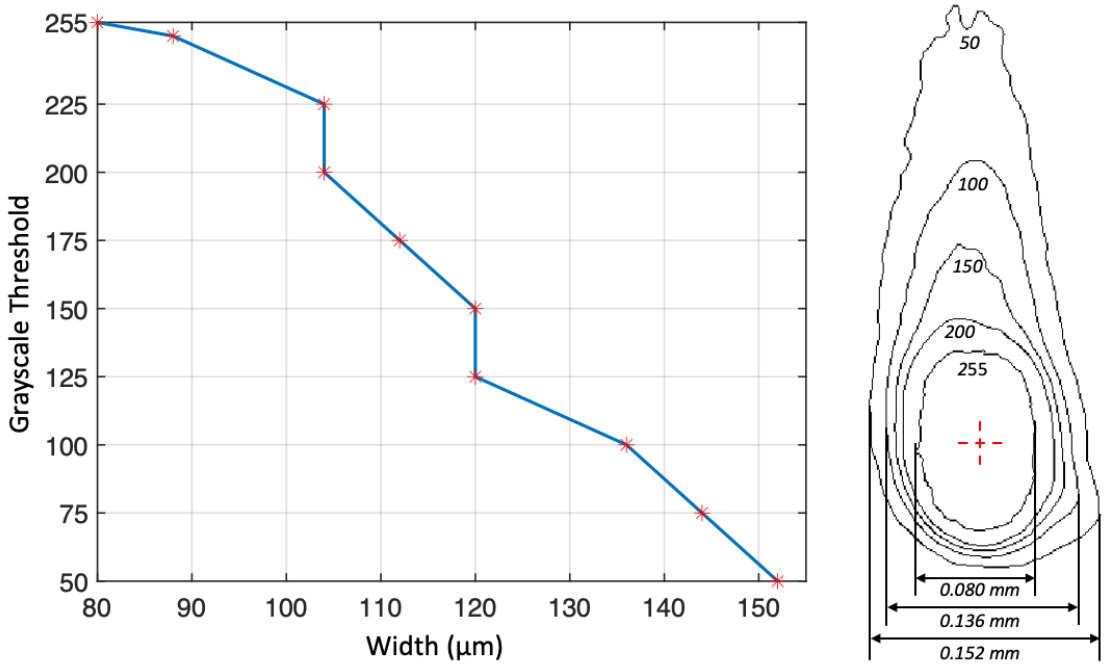

Figure 6. Melt pool width measurement based on different threshold value (left). A melt pool moving vertically from top to bottom. The contour represents the melt pool outline based on different threshold grayscale value. The width represents the widest horizontal length of contour. The intersection of two red dashed lines is the centroid of the area bounded by the 255 value isoline, which could be different to the laser spot center *[34]*.

The key to creating remelting map, in general, is to find the overlapping region between adjacent melting tracks. When a laser beam scans, it not only melts the powder but also remelts the previously solidified tracks. MPM images capture the transient melting status. Figure 7 shows the schematic drawing of the overlapping region between two adjacent tracks, which can be calculated by fusing the registered in-situ MPM data. As shown in the figure, continuously sampled MPM images are aligned to the scan commands to form tracks. f_n^i represents the n_{th} frame of the MPM images at Track i. The track number is extracted from the MPM images registered to the scan path. In the figure, T^1 and T^2 are the first and second melt pool tracks, respectively. The shaded area in red color is the overlapping region in between these two tracks. Note, the thresholding selected in the preprocessing stage can affect the area of the remelting region. However, this paper does not discuss what is the ideal threshold for the most accurate remelting consideration. Instead, it focuses on comparing differences of remelting for overhang and non-overhang surfaces as the same threshold applied on the whole part.

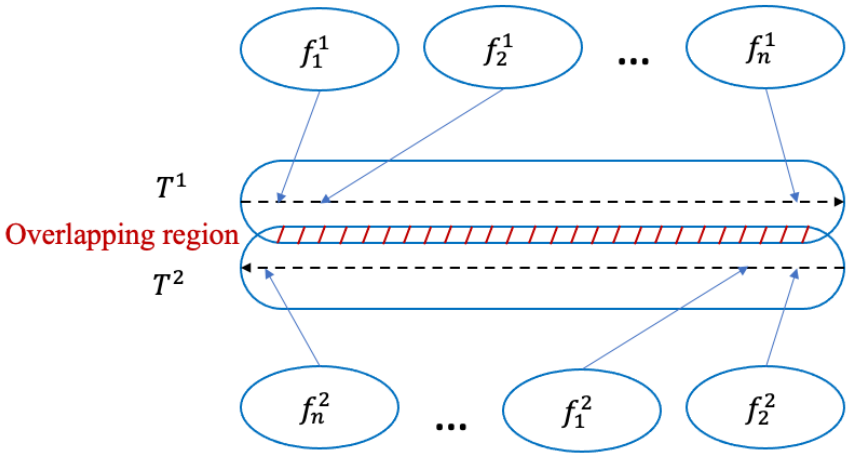

Figure 7. Overlapping region derived from MPM data registration and fusion.

After constructing the remelting map for the entire layer using MPM images, a remelting index is calculated. Equation (1) shows how the remelting ratio is defined. Note, due to the limitation of measurement technique, this paper cannot calculate the remelting overlay area along depth direction. This value indicates the proportion at which all the tracks are overlapped. A higher value indicates that tracks have strongly connected but may also suggests overheating. If this value is too small, it means that the part may suffer from "lack-of-fusion" defects.

$$\varphi = \frac{A_o}{A_p} \tag{1}$$

where φ is the ratio of the overlapping area A_o (green area in Figure 7), and total covered area by all tracks A_p. The ratio is dependent on the melt pool threshold selected during the preprocessing stage. A higher threshold value would lead to lager melt pool area, which cause increment in both A_o and A_p. For fixed hatching distance with multiple tracks, higher threshold value would produce a lower φ. For demonstrative purpose, this paper selects a relatively higher threshold value, 80, for all analysis. The following paragraphs would not further discuss this topic due to the lack of information about MPM image grayscale to melt pool width calibration.

Result

A total of four parts are built in the experiment [28]. The result presented in this paper is based on Part 1 and the complete overhang layers.

Figure 8 shows a magnification of the remelting map for a regular layer (Layer 2) without an overhang from the top left corner (Track 1 and 2) and middle right (Track 26 and 27). The laser beam moves from right to left to create Track 1 and Track 27, where Track 2 and Track 26 are from the opposite direction under Track 1. Fused the registered MPM images create the outline of the melting tracks. The green shaded area is the overlapping region between the two tracks, namely the remelting of Track 1 and 2. The middle figure plots the remelting map for the entire layer and the colormap marks the map from no melting (white) to 3 times remelting. 0 indicates the powder has been melted once but without further remelting. As shown, the majority of the map has a maximum one-time remelting. A few small spots are the area remelted twice caused by several oversized melt pools.

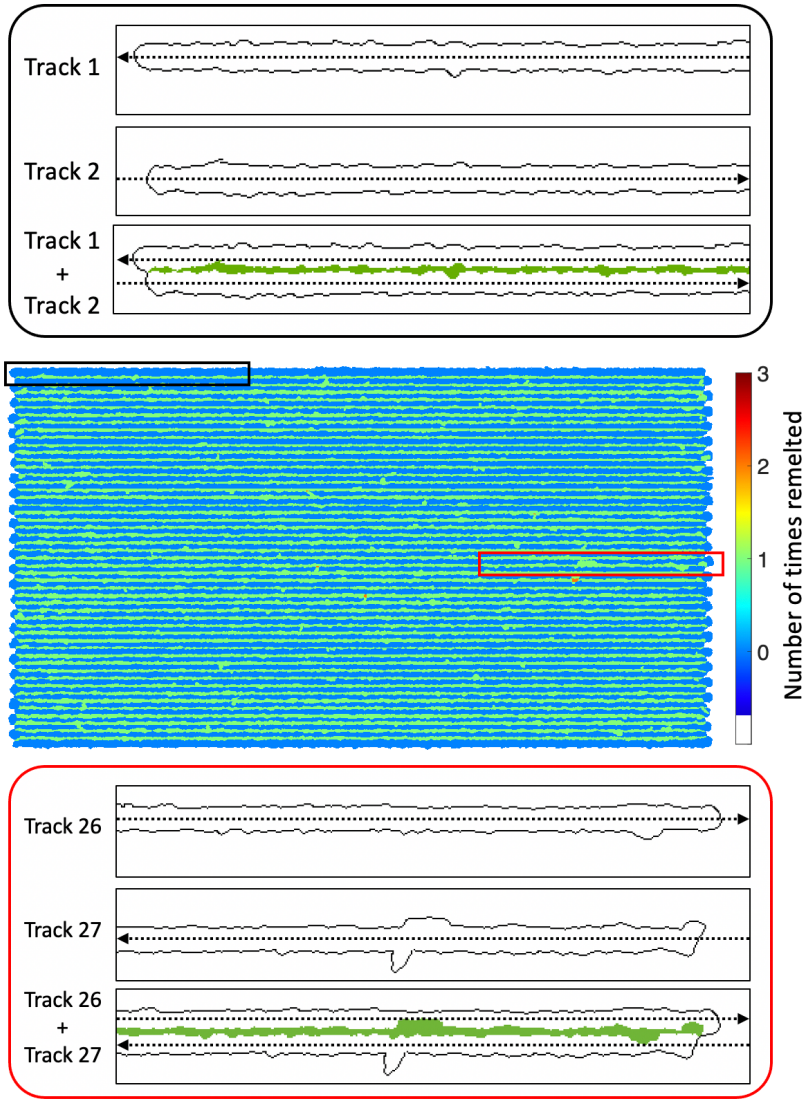

Figure 8. The remelting map between Track 1 and Track 2 (top), and Track 26 and Track 27 (bottom). The remelting map of the entire layer (middle).

Table 2 selects the same region on different layers for comparison, where the scan pattern, size, and location are the same. Layer 226 is the only layer in part that has a complete overhanging region (0.55 mm × 3 mm). The cropped portion is built upon 200 layers of powders. Layer 10 is a regular layer without overhanging feature as a reference. Layer 250 is the last layer of the part. They use the colormap as Figure 8, where the white area indicates the powders not being melted. The last column lists the registered LWI at the same region of each layer. There is no significant difference observed between Layer 10 and 250. However, the remelting in Layer 226 is much lower, and the corresponding LWI seems very blurry without noticeable horizontal stripes.

The remelting maps visually compare the melting conditions within a region which transitions from overhang to subsequent regular layers. Figure 9 aims to describe the impact from overhang features statistically by eight layers from the first overhang layer. The results are based on the same region of each layer as shown in Table 2. The red dots mark the average remelting index calculated from each layer corresponding the overhang region, and subsequent layers above this region. The open circles show the average remelting index of the entire infilling region from Layer 1 to Layer 25, with error bars indicating ±1 standard deviation. Those 25 layers has rectangular outline without overhang introduced. The lower and upper bounds are also plotted. As shown, the number decreased significantly for the immediate overhanging layer from 27.5% in layer 227, to 8.4% in layer

226. The actual overhang surface is geometrically eliminated from Layer 227. However, the same region remains under remelting. It was built upon post overhang surfaces. The light blue bars plot the absolute difference between the overhang region to non-overhang region on current layer. The difference of φ between overhang region and non-overhang region on Layer 226 is 15.2%. Based on the data, it takes three layers to recover the remelting ratio back to the normal range.

Table 2. Remelting map and corresponding LWI for the same region on different layers.

Layer num	Scan direction	Description	Remelting map for overhang region	LWI at the same region
10	H-T2B	One regular layer	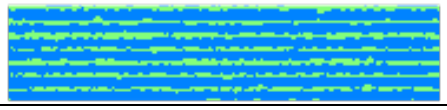	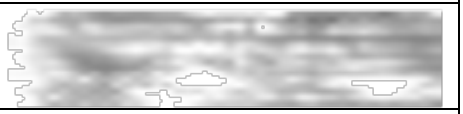
226	H-T2B	First overhang layer		
250	H-T2B	25th regular layer above overhang	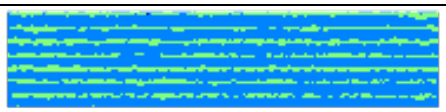	

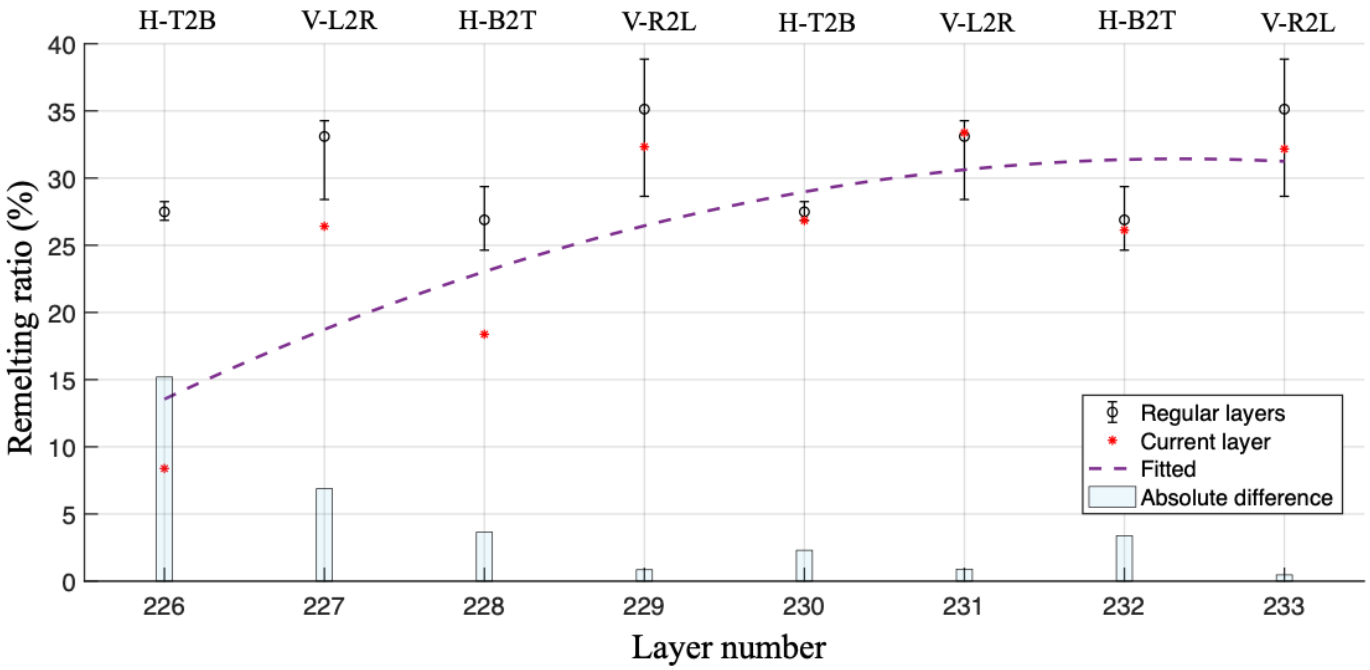

Figure 9. The φ from Layer 226 to Layer 233 of the overhang region cropped from each layer. Red dots mark the φ in current layer. Error bar represents the average remelting range for regular layers with the same scan pattern. The purple curve is the fitted average remelting ratio for Layer 226 to 233, which shows the recovering trend after overhang. The light blue bars are the absolute differences between overhang region and non-overhang region on current layer.

Figure 10 compares an X-ray Computer Tomography (XCT) slice from volume data and remelting map of Layer 226. For clarification, the XCT slice is the preliminary result that taken approximately around 4.500 mm to 4.540 mm in Z direction, which roughly corresponds to layer 226. As shown, the dashed line circles the same region on this layer. The remelting map clearly shows the low overlapping between tracks. Similarly, the XCT scan shows this region has different grayscale than the area without overhang. Note, the darkness of radiographic

density in the X-Ray image is usually affected by sample transmitted density. It is reasonable to assume this region has relative lower density than normal value.

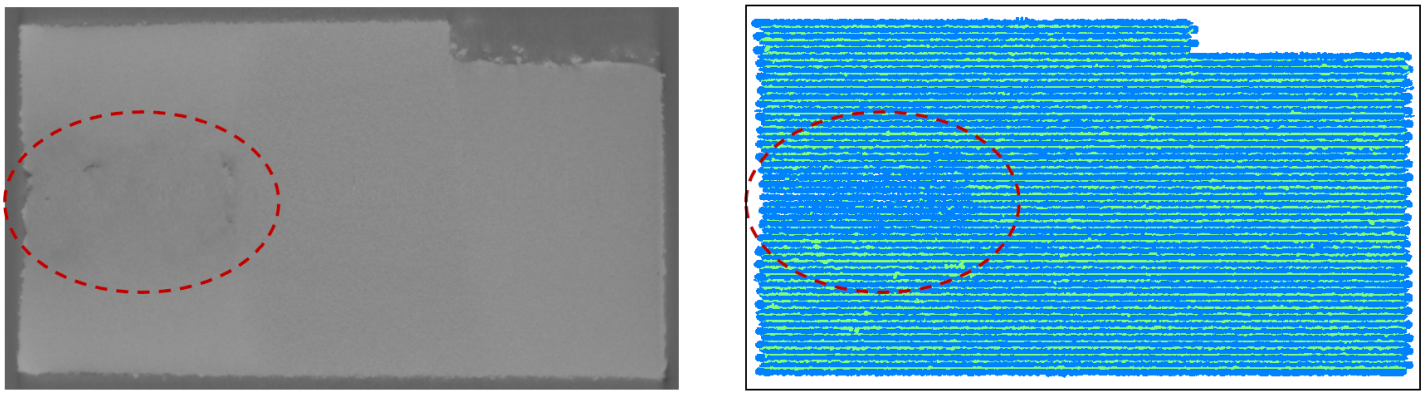

(a) (b)

Figure 10. Comparison between XCT scan and remelting map of Layer 226. (a) is the XCT slice approximately between 4.50 mm to 4.54 mm in Z direction. (b) is the complete remelting map of Layer 226.

Conclusion and Discussion

This paper develops a method to calculate the remelting map based on AM data fusion techniques. The parts with overhanging surfaces were built to verify the method. The result shows the remelting ratio of overhang surfaces is significantly lower than the average of regular layers. An important finding is the irregular remelting conditions would not immediately recover in post-overhanging surface. The following layers remain a lower remelting ratio. To receive full support, the part takes 3 layers to build the strength. The remelting ratio above the overhang region increases from layer to layer to approach that of the non-overhang regions. The proposed method has limitation in precise validation and remelting between layers.

Future research will continue to investigate the physical changes caused by overhanging features, where this paper presents an expected result for complete overhang surfaces. It could be valuable to analyze the conditions for those “mild” overhanging surfaces. Data fusion can expand to multi-modal (MPM and LWI) and deep correlation between remelting ratio and part quality (porosity and surface roughness). Future research would also investigate the most appropriate threshold value to find the melt pool outline. This step may potentially improve the accuracy of remelting ratio. One ongoing research from the coauthor is the recovering scan strategy. This strategy aims to use a near real-time control method to adjust such scan strategy as laser power and spot size in the next layer to fix the remelting issues on current layer.

Disclaimer

Certain commercial systems are identified in this paper. Such identification does not imply recommendation or endorsement by NIST; nor does it imply that the products identified are necessarily the best available for the purpose. Further, any opinions, findings, conclusions, or recommendations expressed in this material are those of the authors and do not necessarily reflect the views of NIST or any other supporting U.S. government or corporate organizations.

Acknowledgments

This material is based upon work supported by the National Institute of Standards and Technology (NIST) under Cooperative Agreement number NIST 70NANB18H258.

References

[1] Babuska, T. F., Krick, B. A., Susan, D. F., 2021, "Comparison of Powder Bed Fusion and Directed Energy Deposition for Tailoring Mechanical Properties of Traditionally Brittle Alloys," Manufacturing Letters, **28**pp. 30-34.

[2] Lopez, F., Witherell, P., and Lane, B., 2016, "Identifying Uncertainty in Laser Powder Bed Fusion Additive Manufacturing Models," Journal of Mechanical Design, **138**(11) .

[3] Arısoy, Y. M., Criales, L. E., Özel, T., 2017, "Influence of Scan Strategy and Process Parameters on Microstructure and its Optimization in Additively Manufactured Nickel Alloy 625 Via Laser Powder Bed Fusion," The International Journal of Advanced Manufacturing Technology, 90(5) pp. 1393-1417.

[4] Yang, Z., Lu, Y., Yeung, H., 2020, "From Scan Strategy to Melt Pool Prediction: A Neighboring-Effect Modeling Method," Journal of Computing and Information Science in Engineering, 20(5) .

[5] Chen, H., Gu, D., Xiong, J., 2017, "Improving Additive Manufacturing Processability of Hard-to-Process Overhanging Structure by Selective Laser Melting," Journal of Materials Processing Technology, 250pp. 99-108.

[6] Yeung, H., Yang, Z., and Yan, L., 2020, "A Meltpool Prediction Based Scan Strategy for Powder Bed Fusion Additive Manufacturing," Additive Manufacturing, 35pp. 101383.

[7] Yeung, H., and Lane, B., 2020, "A Residual Heat Compensation Based Scan Strategy for Powder Bed Fusion Additive Manufacturing," Manufacturing Letters, 25pp. 56-59.

[8] Yeung, H., Lane, B., and Fox, J., 2019, "Part Geometry and Conduction-Based Laser Power Control for Powder Bed Fusion Additive Manufacturing," Additive Manufacturing, 30pp. 100844.

[9] Patel, S., and Vlasea, M., 2020, "Melting Modes in Laser Powder Bed Fusion," Materialia, 9pp. 100591.

[10] Sun, S., Brandt, M., and Easton, M., 2017, "Powder Bed Fusion Processes: An Overview," Laser Additive Manufacturing, pp. 55-77.

[11] Yang, Z., Lu, Y., Li, S., Li, "IN-PROCESS DATA FUSION FOR PROCESS MONITORING AND CONTROL OF METAL ADDITIVE MANUFACTURING," International Design Engineering Technical Conferences and Computers and Information in Engineering Conference, Anonymous ASME, .

[12] Tang, M., Pistorius, P. C., and Beuth, J. L., 2017, "Prediction of Lack-of-Fusion Porosity for Powder Bed Fusion," Additive Manufacturing, 14pp. 39-48.

[13] Tenbrock, C., Fischer, F. G., Wissenbach, K., 2020, "Influence of Keyhole and Conduction Mode Melting for Top-Hat Shaped Beam Profiles in Laser Powder Bed Fusion," Journal of Materials Processing Technology, 278pp. 116514.

[14] Kok, Y., Tan, X. P., Wang, P., 2018, "Anisotropy and Heterogeneity of Microstructure and Mechanical Properties in Metal Additive Manufacturing: A Critical Review," Materials & Design, 139pp. 565-586.

[15] Yang, Z., Lu, Y., Yeung, H., 2020, "3D Build Melt Pool Predictive Modeling for Powder Bed Fusion Additive Manufacturing," International Design Engineering Technical Conferences and Computers and Information in Engineering Conference, Anonymous American Society of Mechanical Engineers, 83983, pp. V009T09A046.

[16] Yadroitsev, I., and Smurov, I., 2010, "Selective Laser Melting Technology: From the Single Laser Melted Track Stability to 3D Parts of Complex Shape," Physics Procedia, 5pp. 551-560.

[17] Fox, J. C., Moylan, S. P., and Lane, B. M., 2016, "Effect of Process Parameters on the Surface Roughness of Overhanging Structures in Laser Powder Bed Fusion Additive Manufacturing," Procedia Cirp, 45pp. 131-134.

[18] Wang, D., Yang, Y., Yi, Z., 2013, "Research on the Fabricating Quality Optimization of the Overhanging Surface in SLM Process," The International Journal of Advanced Manufacturing Technology, 65(9-12) pp. 1471-1484.

[19] Calignano, F., 2014, "Design Optimization of Supports for Overhanging Structures in Aluminum and Titanium Alloys by Selective Laser Melting," Materials & Design, **64**pp. 203-213.

[20] Cheng, B., and Chou, K., 2015, "Geometric Consideration of Support Structures in Part Overhang Fabrications by Electron Beam Additive Manufacturing," Computer-Aided Design, **69**pp. 102-111.

[21] Yang, Y. P., Jamshidinia, M., Boulware, P., 2018, "Prediction of Microstructure, Residual Stress, and Deformation in Laser Powder Bed Fusion Process," Computational Mechanics, 61(5) pp. 599-615.
[22] Mani, M., Feng, S., Brandon, L., 2017, "Measurement science needs for real-time control of additive manufacturing powder-bed fusion processes," CRC Press, .
[23] Feng, S. C., Lu, Y., Jones, A. T., 2021, "Additive Manufacturing in-Situ and Ex-Situ Data Registration and Metadata Definition," Journal of Computing and Information Science in Engineering, .
[24] Lu, Y., Yang, Z., Kim, J., "Camera-Based Coaxial Melt Pool Monitoring Data Registration for Laser Powder Bed Fusion Additive Manufacturing," .
[25] Lane, B., Mekhontsev, S., Grantham, S., 2016, "Design, developments, and results from the NIST additive manufacturing metrology testbed (AMMT)," Solid Freeform Fabrication (SFF) Symposium, Anonymous pp. 1145-1160.
[26] Yeung, H., Lane, B. M., Donmez, M. A., 2018, "Implementation of Advanced Laser Control Strategies for Powder Bed Fusion Systems," Procedia Manufacturing, 26pp. 871-879.
[27] Scime, L., Siddel, D., Baird, S., 2020, "Layer-Wise Anomaly Detection and Classification for Powder Bed Additive Manufacturing Processes: A Machine-Agnostic Algorithm for Real-Time Pixel-Wise Semantic Segmentation," Additive Manufacturing, 36pp. 101453.
[28] Lane, B., and Yeung, H., 2020, "Process Monitoring Dataset from the Additive Manufacturing Metrology Testbed (AMMT): Overhang Part X4," Journal of Research of the National Institute of Standards and Technology, 125pp. 1-18.
[29] Feng, S. C., Lu, Y., and Jones, A. T., 2020, "Measured Data Alignments for Monitoring Metal Additive Manufacturing Processes Using Laser Powder Bed Fusion Methods," International Design Engineering Technical Conferences and Computers and Information in Engineering Conference, Anonymous American Society of Mechanical Engineers, 83983, pp. V009T09A022.
[30] Hall, D. L., and Llinas, J., 1997, "An Introduction to Multisensor Data Fusion," Proceedings of the IEEE, 85(1) pp. 6-23.
[31] Lu, Y., Yang, Z., Eddy, D., "Self-improving additive manufacturing knowledge management," Asme 2018 international design engineering technical conferences and computers and information in engineering conference, Anonymous American Society of Mechanical Engineers Digital Collection, .
[32] Lane, B., Jacquemetton, L., Piltch, M., 2020, "Thermal Calibration of Commercial Melt Pool Monitoring Sensors on a Laser Powder Bed Fusion System," .
[33] Lane, B., and Yeung, H., 2019, "Process Monitoring Dataset from the Additive Manufacturing Metrology Testbed (AMMT):" Three-Dimensional Scan Strategies"," Journal of Research of the National Institute of Standards and Technology, 124pp. 1-14.
[34] Zhirnov, I., Mekhontsev, S., Lane, B., 2020, "Accurate Determination of Laser Spot Position during Laser Powder Bed Fusion Process Thermography," Manufacturing Letters, 23pp. 49-52.